PHYSICAL REVIEW E **92**, 023201 (2015)

Averaged model for momentum and dispersion in hierarchical porous media

Morgan Chabanon,[1,2,3,*] Bertrand David,[2] and Benoît Goyeau[3,†]
[1]*Mechanical and Aerospace Engineering, University of California San Diego, La Jolla, California 92093, USA*
[2]*MSSMat, UMR-CNRS 8579, Ecole Centrale Paris, Grande Voie des Vignes, 92295 Châtenay-Malabry, France*
[3]*EM2C, UPR-CNRS 288, Ecole Centrale Paris, Grande Voie des Vignes, 92295 Châtenay-Malabry, France*
(Received 22 February 2015; revised manuscript received 8 June 2015; published 3 August 2015)

Hierarchical porous media are multiscale systems, where different characteristic pore sizes and structures are encountered at each scale. Focusing the analysis to three pore scales, an upscaling procedure based on the volume-averaging method is applied twice, in order to obtain a macroscopic model for momentum and diffusion-dispersion. The effective transport properties at the macroscopic scale (permeability and dispersion tensors) are found to be explicitly dependent on the mesoscopic ones. Closure problems associated to these averaged properties are numerically solved at the different scales for two types of bidisperse porous media. Results show a strong influence of the lower-scale porous structures and flow intensity on the macroscopic effective transport properties.

DOI: 10.1103/PhysRevE.92.023201 PACS number(s): 45.20.−d, 47.56.+r

I. INTRODUCTION

Porous systems often exhibit hierarchical configurations, where for instance the solid matrix at the mesoscopic scale is itself microporous. Another example concerns porous media where the impermeable solid mesostructure is embedded in a finer saturated porous medium, itself eventually embedded in another finer porous structure, and so on (see Fig. 1). In other words, the pores at a given scale are filled with a finer porous medium with a structure that is not necessarily the same as the structure at the upper scale.

This type of *hierarchical* porous media has been characterized using several terminologies depending on the number of scales and the associated porous morphologies. For example, two-scale porous structures composed of spherical solid particles are described as "binary mixture" [1], "multisized" porous media [2–4], "bimodal" distribution of particles [5,6], or "bidisperse" [7,8]. This latter terminology has been widely used to describe transfer phenomena in catalyst pellets where the porous architecture is represented by micro- and macropore network, the terminology "bidisperse" being in that case the dispersion of the pore size instead of the grain size [9–11].

Although these multiscale porous structures are present in a large variety of applications (packed-bed reactors, sandy soils,...), few attempts have been performed in order to propose averaged models taking into account the hierarchical dependence on the geometry and the physics at the different scales of the system. Part of the studies have been devoted to the determination of the permeability. Modified expression of the Kozeny-Carman relationship have been obtained for porous structures composed of multisized spherical particles [1–3,8] or for bimodal fibrous porous media [6,12]. Moutsopoulos and Koch [7] considered a bidiperse porous medium composed of spheres of two different characteristic length scales. Using ensemble averaging they showed that the smaller grains have higher influence on the permeability, while large grains have a stronger effect on dispersive phenomena. The contribution of the mass transfer boundary layer on the effective dispersion at the larger scale was emphasized. Yet, one limitation of their work is that the theory for moderate and highly permeable media were developed separately.

The objective of the present study is to derive a general macroscopic model for momentum and solute dispersion in a hierarchical porous structure featuring several intermediate scales. For the sake of conciseness, the analysis is here performed on a three-scale hierarchical porous configuration such as the one represented in Fig. 1. Two upscalings are carried out using the volume-averaging method [13]. The effective transport properties (permeability, diffusion-dispersion coefficient) at the largest scale are found to be explicitly dependent on the intermediate and smaller geometrical characteristics and physical phenomena. Note that similar analyses have been performed in the context of large-scale averaging of heterogeneous porous media for momentum [14–17] and solute transport [18–21]. However, the present work differs from the above-cited references in two main points. First, as previously mentioned, the hierarchical porous structures considered here are characterized by impermeable solid matrix embedded in finer porous region. Second, momentum transport is governed by the Darcy-Brinkman equation, allowing to represent high mesoscale permeability values. This leads to nonuniform velocity fields at the intermediate scale, giving rise to nonlinear closure problems for the determination of the macroscopic transport properties. Nevertheless, although different, the analysis for solute dispersion is based on a similar spatial decomposition of the effective diffusion-dispersion coefficient at the mesoscopic scale [18,19]. Numerical results illustrate the dependence of the macroscopic effective properties on the micro- and mesoscale phenomena.

II. DERIVATION OF THE MESOSCALE MODEL

The hierarchical multiscale porous structure under consideration is represented in Fig. 1. At the microscopic scale (scale III) the porous structure is composed of a rigid and inert solid matrix (κ-phase) saturated by a newtonian fluid (α-phase). The porous medium is assumed to be homogeneous, and the physical properties of both the fluid and solid phases

*mchabanon@ucsd.edu
†benoit.goyeau@ecp.fr

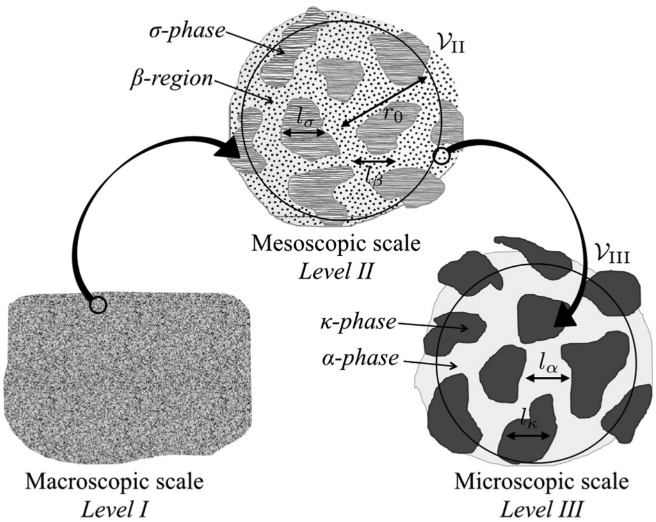

FIG. 1. Representation of the hierarchical porous medium and definition of the different regions.

are constant. In addition, the flow is supposed to be laminar and incompressible. Therefore, at scale III, the conservation equations for momentum and mass of a species A take the classical form

$$\nabla \cdot \mathbf{v}_\alpha = 0, \tag{1}$$

$$\rho_\alpha \frac{\partial \mathbf{v}_\alpha}{\partial t} = -\nabla p_\alpha + \rho_\alpha \mathbf{g} + \mu_\alpha \nabla^2 \mathbf{v}_\alpha, \tag{2}$$

$$\mathbf{v}_\alpha = 0 \quad \text{at } A_{\alpha\kappa}, \tag{3}$$

$$\frac{\partial c_{A\alpha}}{\partial t} + \mathbf{v}_\alpha \cdot \nabla c_{A\alpha} = \nabla \cdot (\mathcal{D}_{A\alpha} \nabla c_{A\alpha}), \tag{4}$$

$$-\mathbf{n}_{\alpha\kappa} \cdot (\mathcal{D}_{A\alpha} \nabla c_{A\alpha}) = 0 \quad \text{at } A_{\alpha\kappa}, \tag{5}$$

where $\mathbf{v}_\alpha$, p_α, and $c_{A\alpha}$ are, respectively, the velocity, pressure, and concentration in the α-phase. ρ_α, μ_α, and $\mathcal{D}_{A\alpha}$ are the density, the dynamic viscosity, and the molecular diffusivity coefficient of the α-phase, while $\mathbf{g}$ is the gravity. Equations (3) and (5) are boundary conditions representing, respectively, no-slip and no-species flux at the fluid-solid interface $A_{\alpha\kappa}$, and $\mathbf{n}_{\alpha\kappa}$ is the unit normal vector oriented from the α-phase toward the κ-phase.

Averaging the above problem using the volume-averaging method [13] has been largely detailed in the literature [13,22–25], and for conciseness only the resulting mesoscopic model at scale II is provided here,

$$\nabla \cdot \langle \mathbf{v}_\alpha \rangle_\beta = 0, \tag{6}$$

$$\rho_\alpha \varepsilon_\alpha^{-1} \frac{\partial \langle \mathbf{v}_\alpha \rangle_\beta}{\partial t} = -\nabla \langle p_\alpha \rangle_\beta^\alpha - \frac{\mu_\alpha}{\mathbf{K}_\alpha^*} \langle \mathbf{v}_\alpha \rangle_\beta + \mu_\alpha \varepsilon_\alpha^{-1} \nabla^2 \langle \mathbf{v}_\alpha \rangle_\beta + \rho_\alpha \mathbf{g}, \tag{7}$$

$$\frac{\partial \left(\varepsilon_\alpha \langle c_{A\alpha} \rangle_\beta^\alpha \right)}{\partial t} + \langle \mathbf{v}_\alpha \rangle_\beta \cdot \nabla \langle c_{A\alpha} \rangle_\beta^\alpha = \nabla \cdot \left(\mathbf{D}_{A\alpha}^* \cdot \nabla \langle c_{A\alpha} \rangle_\beta^\alpha \right), \tag{8}$$

in which $\langle \mathbf{v}_\alpha \rangle_\beta$ is the superficial averaged velocity defined by

$$\langle \mathbf{v}_\alpha \rangle_\beta = \frac{1}{\mathcal{V}_{\rm III}} \int_{V_\alpha} \mathbf{v}_\alpha \, dV, \tag{9}$$

where $\mathcal{V}_{\rm III}$ is the volume of the averaging volume at scale III, and V_α is the volume of the α-phase within $\mathcal{V}_{\rm III}$. Moreover, $\langle p_\alpha \rangle_\beta^\alpha$ and $\langle c_{A\alpha} \rangle_\beta^\alpha$ are the intrinsic averaged pressure and concentration (see Appendix A for the definitions related to the volume averaging method). Note that the subscript β is used to remind that the different averages are defined in the β-region at scale II. The mesoscopic transport equations [Eqs. (7) and (8)] include two effective parameters of the region β: the permeability tensor $\mathbf{K}_\alpha^*$ and the diffusion-dispersion tensor $\mathbf{D}_{A\alpha}^*$, defined as

$$\varepsilon_\alpha \mathbf{K}_\alpha^{*-1} = -\frac{1}{V_\alpha} \int_{A_{\alpha\kappa}} \mathbf{n}_{\alpha\kappa} \cdot (-\mathbf{b}_\alpha + \nabla \mathbf{B}_\alpha) dA, \tag{10}$$

$$\mathbf{D}_{A\alpha}^* = \mathcal{D}_{A\alpha} \left(\varepsilon_\alpha \mathbf{I} + \frac{1}{\mathcal{V}_{\rm III}} \int_{A_{\alpha\kappa}} \mathbf{n}_{\alpha\kappa} \mathbf{d}_\alpha dA \right) - \langle \tilde{\mathbf{v}}_\alpha \mathbf{d}_\alpha \rangle. \tag{11}$$

Here $\mathbf{B}_\alpha$, $\mathbf{b}_\alpha$, and $\mathbf{d}_\alpha$ are closure variables, which are solutions of the two following closure problems

$$0 = -\nabla \mathbf{b}_\alpha + \nabla^2 \mathbf{B}_\alpha + \varepsilon_\alpha \mathbf{K}_\alpha^{*-1}, \tag{12}$$

$$\nabla \cdot \mathbf{B}_\alpha = 0, \tag{13}$$

$$\mathbf{B}_\alpha = -\mathbf{I} \quad \text{at } A_{\alpha\kappa}, \tag{14}$$

$$\mathbf{B}_\alpha(\mathbf{x}) = \mathbf{B}_\alpha(\mathbf{x} + l_i) \quad i = 1,2,3, \tag{15}$$

$$\mathbf{b}_\alpha(\mathbf{x}) = \mathbf{b}_\alpha(\mathbf{x} + l_i) \quad i = 1,2,3, \tag{16}$$

$$\langle \mathbf{b}_\alpha \rangle^\alpha = 0, \text{ and} \tag{17}$$

$$\tilde{\mathbf{v}}_\alpha + \mathbf{v}_\alpha \cdot \nabla \mathbf{d}_\alpha = \mathcal{D}_{A\alpha} \nabla^2 \mathbf{d}_\alpha, \tag{18}$$

$$-\mathbf{n}_{\alpha\kappa} \cdot \nabla \mathbf{d}_\alpha = \mathbf{n}_{\alpha\kappa} \quad \text{at} \quad A_{\alpha\kappa}, \tag{19}$$

$$\mathbf{d}_\alpha(\mathbf{x}) = \mathbf{d}_\alpha(\mathbf{x} + l_i) \quad i = 1,2,3, \tag{20}$$

$$\langle \mathbf{d}_\alpha \rangle^\alpha = 0. \tag{21}$$

It is worth recalling that these problems have been derived under the constraints of spatial and time-scale separations [26]. Equations (15), (16), and (20) are periodic conditions, while Eqs. (17) and (21) provide the uniqueness of the solutions. In order to determine the effective transport properties at scale II, these closure problems are solved numerically using Comsol Multiphysics Software. The numerical validation of the determination of the permeability, not reported here, has been performed by comparing the numerical results with the analytic solution provided by Zick and Homsy [27] for cubic periodic arrays of spheres.

In the following, the analysis is performed on two types of bidimensional periodic unit cells, composed of either inline or staggered arrays of cylinders (Fig. 2). First, the mesoscopic permeability given by Eq. (10) is computed for different values of the porosity ε_α. Since the unit cells considered here are symmetric, the permeability tensor can be reduced to a scalar

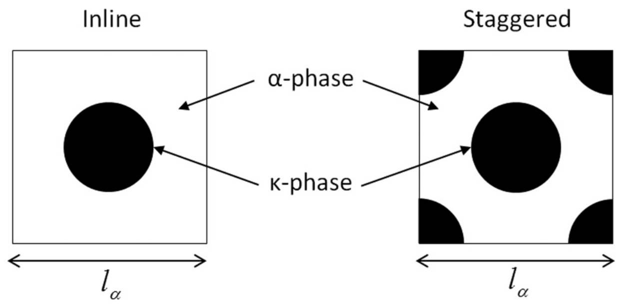

FIG. 2. Inline and staggered periodic unit cells used to solve the closure problems at scale III [Eqs. (12)–(21)] and compute the effective properties in the β-region.

such as $K_\alpha^* \mathbf{I}$. The dimensionless mescoscopic permeabilities are depicted in Fig. 3 for the two unit cells. As expected, the values of the permeability increase with the porosity, and a factor two is observed between the inline and staggered configurations. Then, the diffusion-dispersion tensor, defined by Eq. (11), is computed as a function of the solutal Péclet number, and for three values of the porosity. The longitudinal diffusion-dispersion coefficients for inline and staggered configuration are plotted in Fig. 4. Two classical regions are observed: at small Péclet numbers, species transport is mainly driven by diffusion, while dispersion process strongly dominates at large Péclet. Note that the shift between the two regimes depends on the arrangement of the microstructure. Indeed, this transition takes place at a larger range of Péclet for the staggered configuration, and the longitudinal coefficient is found to be one order of magnitude smaller than for the inline structure. This is mainly due to the fact that, in this latter case, dispersion occurs primarily in the direction of the flow, while transverse dispersion is found to be important for more tortuous staggered structures [25].

III. DERIVATION OF THE MACROSCALE MODEL

Although standard, the above preliminary upscaling is primordial since it establishes the local physics in the β-region

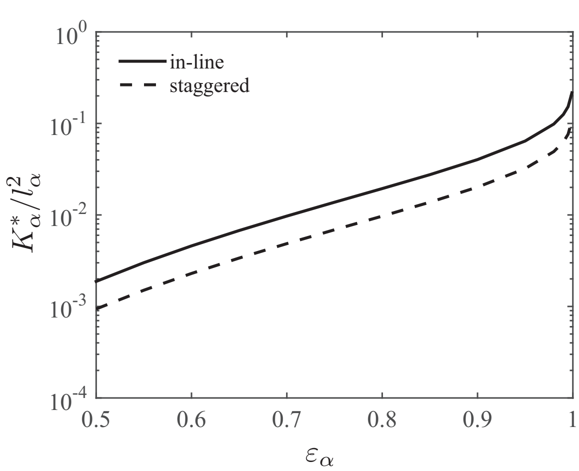

FIG. 3. Computed dimensionless permeability for inline and staggered cylinders, as a function of the microscale permeability.

at scale II. Before performing the second upscaling, in order to simplify the notations, the following nomenclature is adopted

$$\mathbf{v}_\beta = \langle \mathbf{v}_\alpha \rangle_\beta, \tag{22}$$

$$p_\beta = \langle p_\alpha \rangle_\beta^\alpha, \tag{23}$$

$$c_{A\beta} = \langle c_{A\alpha} \rangle_\beta. \tag{24}$$

Note that $\mathbf{v}_\beta$ and $c_{A\beta}$ are superficial averages, while p_β is an intrinsic average. The above notations allow us to rewrite the transport equations in the β-region [Eqs. (6)–(8)] as

$$\nabla \cdot \mathbf{v}_\beta = 0 \quad \text{in the } \beta\text{-region}, \tag{25}$$

$$\begin{aligned} \rho_\alpha \varepsilon_\alpha^{-1} \frac{\partial \mathbf{v}_\beta}{\partial t} &= -\nabla p_\beta - \frac{\mu_\alpha}{\mathbf{K}_\alpha^*} \mathbf{v}_\beta + \mu_\alpha \varepsilon_\alpha^{-1} \nabla^2 \mathbf{v}_\beta \\ &\quad + \rho_\alpha \mathbf{g} \quad \text{in the } \beta\text{-region}, \end{aligned} \tag{26}$$

$$\varepsilon_\alpha \frac{\partial c_{A\beta}}{\partial t} + \mathbf{v}_\beta \cdot \nabla c_{A\beta} = \nabla \cdot (\mathbf{D}_{A\alpha}^* \cdot \nabla c_{A\beta}) \quad \text{in the } \beta\text{-region}. \tag{27}$$

It is important to keep in mind that the effective dispersion tensor $\mathbf{D}_{A\alpha}^*$ depends nonlinearly on the value of the cell Péclet number defined as

$$\mathrm{Pe}_\alpha = \frac{\|v_\alpha\| l_\alpha}{\mathcal{D}_{A\alpha}}, \tag{28}$$

where

$$\|v_\alpha\| = \left(\langle \mathbf{v}_\alpha \rangle_\beta^\alpha \cdot \langle \mathbf{v}_\alpha \rangle_\beta^\alpha \right)^{1/2} = \varepsilon_\alpha^{-1} (\mathbf{v}_\beta \cdot \mathbf{v}_\beta)^{1/2}, \tag{29}$$

and therefore on the mesoscopic velocity field. Consequences on the derivation of the macroscopic solute transport are detailed in Sec. III B.

Before proceeding to the upscaling from scale II to I, let us define the boundary conditions at the porous-solid interface $A_{\beta\sigma}$. Strictly speaking, boundary conditions at the interface between a porous layer and an homogeneous plain phase (fluid or solid) should result from upscaling the local transport phenomena in this interfacial region. This has been the object of intense research activity for transport modeling at a fluid-porous interface through the so-called Beavers and Joseph's problem [28–31], but the equivalent for transport phenomena between a fluid and a solid is still missing. In the present analysis, since momentum transport is governed by the Darcy-Brinkman equation, and due to the fact that the larger solid matrix is impermeable, a no-slip condition and a null diffusive flux are considered at $A_{\beta\sigma}$:

$$\mathbf{v}_\beta = 0 \quad \text{at } A_{\beta\sigma}, \tag{30}$$

$$\mathbf{n}_{\beta\sigma} \cdot (\mathbf{D}_{A\alpha}^* \cdot \nabla c_{A\beta}) = 0 \quad \text{at } A_{\beta\sigma}. \tag{31}$$

Equations (25)–(27), with the boundary condition Eqs. (30) and (31), represent the local system at the mesoscopic scale (scale II). In order to derive macroscopic transport equations (scale I), the volume averaging method is applied once more. Note that the form of the system at scale II is similar to the one described at scale III. The main differences are due to the

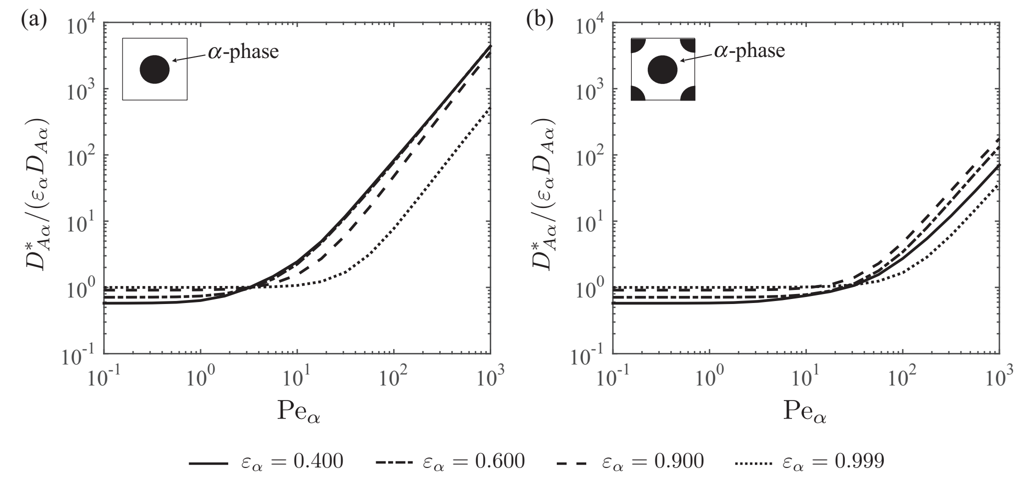

FIG. 4. Dimensionless longitudinal diffusion-dispersion for inline (a) and staggered (b) cylinders, as a function of the mesoscopic Péclet number Pe_α, and for different porosities ε_α.

presence of the Darcy term in Eq. (26) and to the *nonconstant diffusion-dispersion* tensor in Eq. (27).

A. Momentum transport

Applying the averaging procedure to Eq. (26) leads to the following nonclosed macroscopic equation,

$$\begin{aligned}\rho_\alpha \varepsilon_\alpha^{-1} \frac{\partial(\varepsilon_\beta \langle \mathbf{v}_\beta \rangle^\beta)}{\partial t} &= -\varepsilon_\beta \nabla \langle p_\beta \rangle^\beta - \frac{\mu_\alpha}{\mathbf{K}_\alpha^*} \varepsilon_\beta \langle \mathbf{v}_\beta \rangle^\beta + \mu_\alpha \varepsilon_\alpha^{-1} \varepsilon_\beta \nabla^2 \langle \mathbf{v}_\beta \rangle^\beta \\ &\quad + \varepsilon_\beta \rho_\alpha \mathbf{g} + \frac{1}{\mathcal{V}_{\mathrm{II}}} \int_{A_{\beta\sigma}} \mathbf{n}_{\beta\sigma} \cdot \left(-\mathbf{I}\tilde{p}_\beta + \mu_\alpha \varepsilon_\alpha^{-1} \nabla \tilde{\mathbf{v}}_\beta\right) dA,\end{aligned} \tag{32}$$

where $\tilde{\mathbf{v}}_\beta$ and $\tilde{p}_\beta$ are the spatial deviations of the mesoscopic velocity and the pressure [32], respectively. It is worth mentioning that Eq. (32) is valid under the following length-scale constraints [13]:

$$l_\beta \ll r_0, \tag{33}$$

$$r_0^2 \ll L_\varepsilon L_{p1}, \tag{34}$$

$$r_0^2 \ll L_\varepsilon L_{v1}, \tag{35}$$

$$r_0^2 \ll L_\varepsilon L_{v2}, \tag{36}$$

where l_β is the mesoscopic pore length scale, and r_0 is the size of the averaging volume $\mathcal{V}_{\mathrm{II}}$. L_{p1}, L_{v1}, and L_{v2} represent the characteristic length scales for the macroscopic pressure gradient, velocity gradient, and velocity laplacian, respectively. In order to close Eq. (32), a problem for the deviations $\tilde{\mathbf{v}}_\beta$ and $\tilde{p}_\beta$ must be built. This is done by introducing the spatial deviations into the local problem, and subtracting to it the nonclosed macroscopic equations. This leads to the following deviation problem:

$$\nabla \cdot \tilde{\mathbf{v}}_\beta = 0 \quad \text{in the } \beta\text{-region}, \tag{37}$$

$$\begin{aligned}0 = -\nabla \tilde{p}_\beta - \frac{\mu_\alpha}{\mathbf{K}_\alpha^*} \tilde{\mathbf{v}}_\beta + \mu_\alpha \varepsilon_\alpha^{-1} \nabla^2 \tilde{\mathbf{v}}_\beta - \frac{1}{V_\beta} \int_{A_{\beta\sigma}} \mathbf{n}_{\beta\sigma} \\ \cdot \left(-\mathbf{I}\tilde{p}_\beta + \mu_\alpha \varepsilon_\alpha^{-1} \nabla \tilde{\mathbf{v}}_\beta\right) dA \quad \text{in the } \beta\text{-region},\end{aligned} \tag{38}$$

$$\tilde{\mathbf{v}}_\beta = -\langle \mathbf{v}_\beta \rangle^\beta \quad \text{at } A_{\beta\sigma}. \tag{39}$$

The only source term in this system is given by the boundary condition Eq. (39). In order to link the deviation problem to the nonclosed averaged problem, the form of the source term suggests expressing the deviations as

$$\tilde{\mathbf{v}}_\beta = \mathbf{B}_\beta \cdot \langle \mathbf{v}_\beta \rangle^\beta, \tag{40}$$

$$\tilde{p}_\beta = \mu_\alpha \varepsilon_\alpha^{-1} \mathbf{b}_\beta \cdot \langle \mathbf{v}_\beta \rangle^\beta, \tag{41}$$

where $\mathbf{b}_\beta$ and $\mathbf{B}_\beta$ represent the closure variables. Note the presence of the microscopic porosity in Eq. (41). Substituting the above expressions in the nonclosed averaged momentum Eq. (32) gives

$$\begin{aligned}\rho_\alpha \varepsilon_\alpha^{-1} \varepsilon_\beta^{-1} \frac{\partial(\varepsilon_\beta \langle \mathbf{v}_\beta \rangle^\beta)}{\partial t} &= -\nabla \langle p_\beta \rangle^\beta + \mu_\alpha \varepsilon_\alpha^{-1} \nabla^2 \langle \mathbf{v}_\beta \rangle^\beta + \rho_\alpha \mathbf{g} - \mu_\alpha \varepsilon_\alpha^{-1} \\ &\quad \times \left[\frac{\varepsilon_\alpha}{\mathbf{K}_\alpha^*} - \frac{1}{V_\beta} \int_{A_{\beta\sigma}} \mathbf{n}_{\beta\sigma} \cdot (-\mathbf{I}\mathbf{b}_\beta + \nabla \mathbf{B}_\beta) dA\right] \langle \mathbf{v}_\beta \rangle^\beta.\end{aligned} \tag{42}$$

One can identify a classical form of the permeability tensor depending on the closure variables in the β-region. Thus, if we define

$$\varepsilon_\beta \mathbf{K}_\beta^{*-1} = -\frac{1}{V_\beta} \int_{A_{\beta\sigma}} \mathbf{n}_{\beta\sigma} \cdot (-\mathbf{I}\mathbf{b}_\beta + \nabla \mathbf{B}_\beta) dA, \tag{43}$$

the term in braces in Eq. (42) can be written such as

$$\varepsilon_\alpha \varepsilon_\beta \mathbf{K}_{\mathrm{eff}}^{-1} = \varepsilon_\alpha \mathbf{K}_\alpha^{*-1} + \varepsilon_\beta \mathbf{K}_\beta^{*-1}, \tag{44}$$

where $\mathbf{K}_{\mathrm{eff}}$ represents the effective permeability tensor at the macroscopic scale (scale I). It explicitly involves two contributions: the permeability arising from the microscale

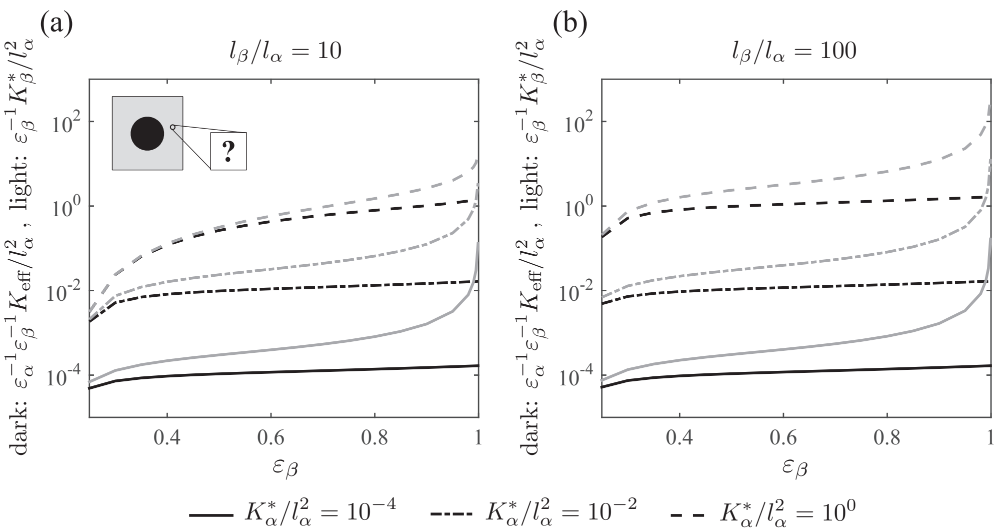

FIG. 5. Nondimensional values of the effective macroscale permeability K_{eff} (black) and mesoscale drag K_β^* (gray), for arbitrarily set mesoscopic permeabilities K_α^* ($\varepsilon_\alpha = 0.6$).

($\mathbf{K}_\alpha^*$) and the drag at the mesoscale ($\mathbf{K}_\beta^*$). Using Eq. (44) into Eq. (42) allows us to express the closed averaged momentum equation in a "Darcy-Brinkman form":

$$\rho_\alpha \varepsilon_\alpha^{-1} \varepsilon_\beta^{-1} \frac{\partial(\varepsilon_\beta \langle \mathbf{v}_\beta \rangle^\beta)}{\partial t} = -\nabla \langle p_\beta \rangle^\beta - \frac{\mu_\alpha}{\mathbf{K}_{\text{eff}}} \varepsilon_\beta \langle \mathbf{v}_\beta \rangle^\beta + \mu_\alpha \varepsilon_\alpha^{-1} \nabla^2 \langle \mathbf{v}_\beta \rangle^\beta + \rho_\alpha \mathbf{g}. \quad (45)$$

If one seeks to take into account a specific structure at the microscale, the determination of the macroscopic permeability must be performed in two steps: first $\mathbf{K}_\alpha^*$ should be obtained by solving the microscopic closure problem [Eqs. (12)–(17)] on a representative periodic unit cell of porosity ε_α. Then, $\mathbf{K}_\beta^*$ should be determined through the resolution of a mesoscopic closure problem, which is obtained by introducing the deviations Eqs. (40) and (41) in the associated deviation problem Eqs. (37)–(39)

$$0 = -\nabla \mathbf{b}_\beta - \varepsilon_\alpha \mathbf{K}_\alpha^{*-1} \mathbf{B}_\beta + \nabla^2 \mathbf{B}_\beta + \varepsilon_\beta \mathbf{K}_\beta^{*-1}, \quad (46)$$

$$\nabla \cdot \mathbf{B}_\beta = 0, \quad (47)$$

$$\mathbf{B}_\beta = -\mathbf{I} \quad \text{at } A_{\beta\sigma}, \quad (48)$$

$$\mathbf{B}_\beta(\mathbf{x}) = \mathbf{B}_\beta(\mathbf{x} + l_i) \quad i = 1,2,3, \quad (49)$$

$$\mathbf{b}_\beta(\mathbf{x}) = \mathbf{b}_\beta(\mathbf{x} + l_i) \quad i = 1,2,3, \quad (50)$$

$$\langle \mathbf{b}_\beta \rangle^\beta = 0. \quad (51)$$

Note that this mesoscopic closure problem explicitly involves the microscopic drag contribution through $\mathbf{K}_\alpha^*$. Therefore, under its present form, this problem is similar to a Darcy-Brinkman flow instead of the classical Stokes flow.

In this document, the length scale associated with the microscale (scale III) is taken as the length of reference to express the dimensionless values of the different permeabilities. Therefore, the ratio between scale II and scale III l_β/l_α is an important parameter to take into account in order to illustrate the influence of the hierarchical structure on the effective transport properties. While a large length-scale separation guaranties the fulfillment of the constraints necessitated by the up-scaling procedure, a smaller length-scale ratio allows us to observe more clearly the hierarchical effects on the transport phenomena. Therefore, all the results below are reported for two length-scale ratios of 10 and 100. Note that a separation of one order of magnitude has been shown to be enough for the up-scaling of momentum transport in porous structures [33].

Numerical results illustrating the hierarchical contribution to the macroscale permeability are presented in Fig. 5. Here, in order to have access to a larger range of parameter values, the couple (ε_α, $\mathbf{K}_\alpha^*$) is arbitrarily set, allowing us to observe more easily the interscale dependency. The effective permeability at scale I, $\mathbf{K}_{\text{eff}}$ (solid lines) and the permeability $\mathbf{K}_\beta^*$ associated to the drag at the mesoscopic scale (dashed lines) are plotted for different values of the permeability in the β-region, and for two ratios of the characteristic cell sizes. Note that the microscopic porosity ε_α is kept equal to 0.6. First, it can be seen that $\mathbf{K}_\alpha^*$ strongly influences the macroscopic permeability coefficient, especially for large values of ε_β where $\mathbf{K}_{\text{eff}}$ tends to $\mathbf{K}_\alpha^*$. On the other hand, we verify that $\mathbf{K}_{\text{eff}}$ logically tends toward $\mathbf{K}_\beta^*$ for small ε_β values and obviously for large $\mathbf{K}_\alpha^*$ (fluid behavior). Note that these observations are verified whatever the length-scale ratio l_β/l_α.

B. Species transport

Let us now turn our attention on the derivation of the macroscopic species transport model and the determination of the associated effective multiscale dispersion coefficient.

The local mass transport at scale II is governed by Eqs. (27) and (31). At first sight, Eq. (27) looks similar to a classical diffusion convection equation, and the derivation of its macroscopic form at scale I using the volume-averaging method seems straight forward. However, the difficulty here lies in the diffusive term, whose effective diffusion-dispersion coefficient $\mathbf{D}_{A\alpha}^*$ depends on the local mesoscopic velocity field

$\mathbf{v}_\beta$ [Eq. (29)]. Such a problem has been treated in the context of heterogeneous porous media by Quintard and Whitaker [15] considering the spatial decomposition of the diffusion-dispersion effective coefficient (see also Refs. [19,21]). In consistence with this idea, the following spatial decomposition is proposed:

$$\mathbf{D}^*_{A\alpha} = \langle \mathbf{D}^*_{A\alpha}\rangle^\beta + \tilde{\mathbf{D}}^*_{A\alpha}, \tag{52}$$

where $\tilde{\mathbf{D}}^*_{A\alpha}$ represents the spatial deviation around the average quantity $\langle \mathbf{D}^*_{A\alpha}\rangle^\beta$. For conciseness, only the main steps of the derivation are reported in this section, with all the details being provided in Appendix B. In addition to Eq. (52), the spatial decompositions of the concentration and velocity fields are introduced, and the nonclosed macroscopic mass transport equation can be written

$$\varepsilon_\alpha \frac{\partial(\varepsilon_\beta \langle c_{A\beta}\rangle^\beta)}{\partial t} + \varepsilon_\beta \langle \mathbf{v}_\beta\rangle^\beta \cdot \nabla \langle c_{A\beta}\rangle^\beta$$
$$= \nabla \cdot \left[\langle \mathbf{D}^*_{A\alpha}\rangle^\beta \cdot \left(\varepsilon_\beta \nabla \langle c_{A\beta}\rangle^\beta + \frac{1}{\mathcal{V}_{\mathrm{II}}} \int_{A_{\beta\sigma}} \mathbf{n}_{\beta\sigma} \tilde{c}_{A\beta} dA \right) \right.$$
$$\left. - \langle \tilde{\mathbf{v}}_\beta \tilde{c}_{A\beta}\rangle \right] + \nabla \cdot \langle \tilde{\mathbf{D}}^*_{A\alpha} \cdot \nabla \tilde{c}_{A\beta}\rangle, \tag{53}$$

where the right-hand side corresponds to the hierarchical contributions to diffusion-dispersion phenomena. The first term, involving the tensor $\langle \mathbf{D}^*_{A\alpha}\rangle^\beta$, represents the averaged diffusion-dispersion at scale II, while the last term is an additional contribution of the dispersion due to the dependence of $\mathbf{D}^*_{A\alpha}$ on the velocity field. Once again, the problem for the deviations is derived by subtracting Eq. (53) from Eq. (27), after having introduced the spatial decompositions. It follows that, providing scale separation and quasistationarity are satisfied, the deviation problem for mass transport takes the form

$$\tilde{\mathbf{v}}_\beta \cdot \nabla \langle c_{A\beta}\rangle^\beta + \mathbf{v}_\beta \cdot \nabla \tilde{c}_{A\beta}$$
$$= \nabla \cdot (\mathbf{D}^*_{A\alpha} \cdot \nabla \tilde{c}_{A\beta}) + \nabla \cdot (\tilde{\mathbf{D}}^*_{A\alpha} \cdot \nabla \langle c_{A\beta}\rangle^\beta) \tag{54}$$
$$-\mathbf{n}_{\beta\sigma} \cdot (\mathbf{D}^*_{A\alpha} \cdot \nabla \tilde{c}_{A\beta}) = \mathbf{n}_{\beta\sigma} \cdot (\mathbf{D}^*_{A\alpha} \cdot \nabla \langle c_{A\beta}\rangle^\beta) \quad \text{at } A_{\beta\sigma}. \tag{55}$$

From the boundary condition Eq. (55), it clearly appears that the two diffusive terms in Eq. (54) are of the same order of magnitude (see Appendix C). Therefore, we are left with second- and third-order source terms. This suggests that the deviation concentration $\tilde{c}_{A\beta}$ might be related to the averaged values as

$$\tilde{c}_{A\beta} = \mathbf{d}_\beta \cdot \nabla \langle c_{A\beta}\rangle^\beta + \phi_\beta \nabla^2 \langle c_{A\beta}\rangle^\beta, \tag{56}$$

where the scalar ϕ_β and vector $\mathbf{d}_\beta$ are closure variables. The introduction of Eq. (56) in Eqs. (54) and (55) would lead to two closure problems, one corresponding to the first-order derivative of $\langle c_{A\beta}\rangle^\beta$ (for $\mathbf{d}_\beta$), the other for the second-order derivative. However, in practice, the expansion at the first order is sufficient to obtain an accurate determination of the effective transport properties [19–21]. Under these considerations, Eq. (56) reduces to

$$\tilde{c}_{A\beta} = \mathbf{d}_\beta \cdot \nabla \langle c_{A\beta}\rangle^\beta, \tag{57}$$

giving rise to the closure problem

$$\tilde{\mathbf{v}}_\beta + \mathbf{v}_\beta \cdot \nabla \mathbf{d}_\beta = \nabla \cdot (\mathbf{D}^*_{A\alpha} \cdot \nabla \mathbf{d}_\beta) + \nabla \cdot \tilde{\mathbf{D}}^*_{A\alpha} \tag{58}$$

$$-\mathbf{n}_{\beta\sigma} \cdot (\mathbf{D}^*_{A\alpha} \cdot \nabla \mathbf{d}_\beta) = \mathbf{n}_{\beta\sigma} \cdot \mathbf{D}^*_{A\alpha} \quad \text{at } A_{\beta\sigma} \tag{59}$$

$$\mathbf{d}_\beta(\mathbf{x}) = \mathbf{d}_\beta(\mathbf{x} + l_i) \quad l_i = 1,2,3 \tag{60}$$

$$\langle \mathbf{d}_\beta\rangle^\beta = 0. \tag{61}$$

Note that a similar form including the additional dispersion term has been obtained for solute transport in heterogeneous

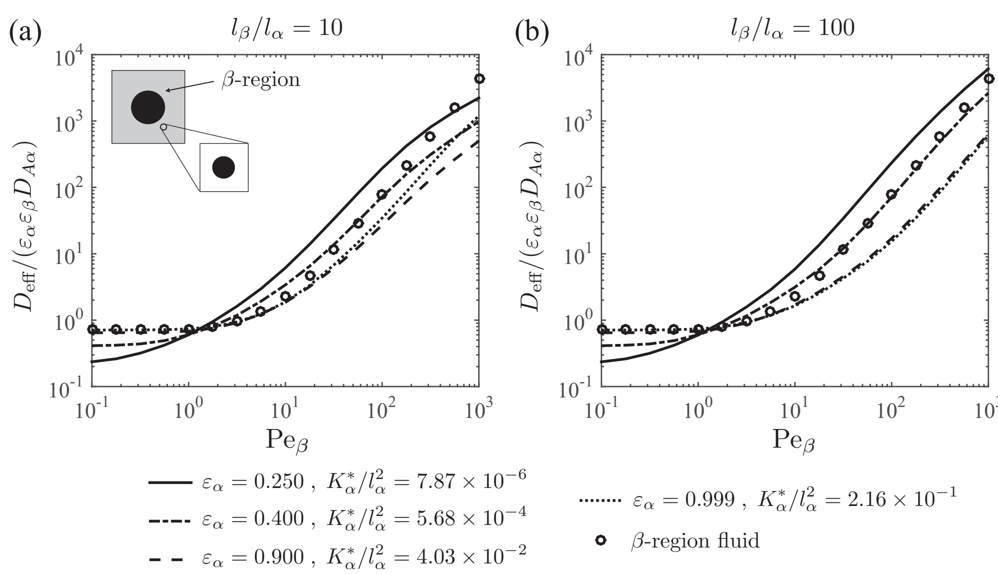

FIG. 6. Nondimensional values of the longitudinal diffusion-dispersion coefficient for a bidisperse structure composed at both scales of inline cylinders ($\varepsilon_\beta = 0.6$).

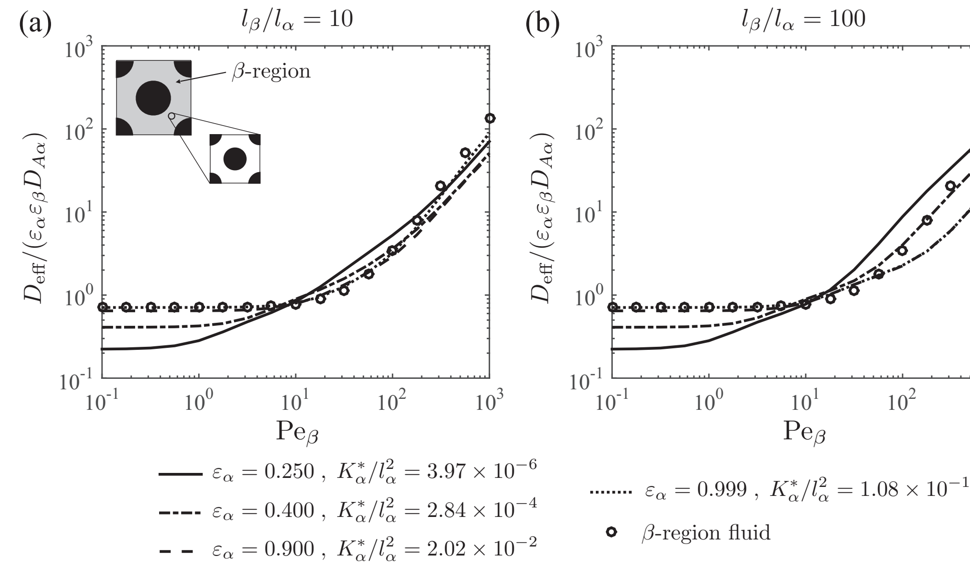

FIG. 7. Nondimensional values of the longitudinal diffusion-dispersion coefficient for a bidisperse structure composed at both scales of staggered cylinders ($\varepsilon_\beta = 0.6$).

porous media [18,19]. However, in these previews studies, because the velocity field was obtained from Darcy's law, the source term involving $\tilde{\mathbf{D}}^*_{A\alpha}$ was neglected. In the present analysis, momentum transport is governed by the Darcy-Brinkman equation [Eq. (26)], resulting in a nonconstant diffusion-dispersion coefficient, which deviations can be significant. Finally, substituting Eq. (57) into Eq. (53) yields to the closed form of the macroscopic conservation equation for mass transport

$$\varepsilon_\alpha \frac{\partial}{\partial t}(\varepsilon_\beta \langle c_{A\beta}\rangle^\beta) + \varepsilon_\beta \langle \mathbf{v}_\beta\rangle^\beta \cdot \nabla \langle c_{A\beta}\rangle^\beta = \nabla\cdot(\mathbf{D}_{\mathrm{eff}}\cdot\nabla\langle c_{A\beta}\rangle^\beta), \tag{62}$$

where the macroscopic diffusion-dispersion tensor is given by

$$\mathbf{D}_{\mathrm{eff}} = \langle \mathbf{D}^*_{A\alpha}\rangle^\beta \cdot \left(\varepsilon_\beta \mathbf{I} + \frac{1}{\mathcal{V}_{\mathrm{II}}}\int_{A_{\beta\sigma}} \mathbf{n}_{\beta\sigma}\mathbf{d}_\beta dA\right) - \langle \tilde{\mathbf{v}}_\beta \mathbf{d}_\beta\rangle + \langle \tilde{\mathbf{D}}^*_{A\alpha}\cdot\nabla\mathbf{d}_\beta\rangle. \tag{63}$$

Let us recall that the $\mathbf{D}^*_{A\alpha}$ is an effective tensor resulting from the upscaling from the micro- to the mesoscopic scale. In Eq. (63), the first and second terms are relatively classic, they represent the mesoscopic contribution to the macroscopic effective diffusion-dispersion coefficient, and the effect of convective transport on dispersion, respectively. The third term, however, is more unusual and is a macroscopic diffusive

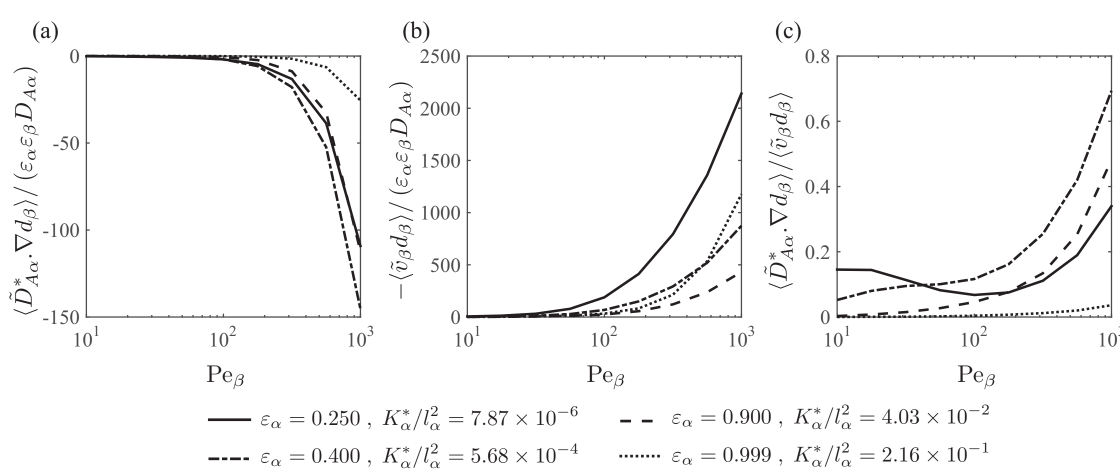

FIG. 8. Contributions of the individual dispersive terms in Eq. (63) as a function of the Péclet, for a bidisperse structure composed at both scales of inline cylinders (scale separation, $l_\beta/l_\alpha = 10$; mesoscopic volume fraction, $\varepsilon_\beta = 0.6$). Dimensionless values of (a) the additional dispersive term arising from the mesocsopic deviation of the diffusion-dispersion tensor, (b) the classical dispersive term, and (c) the ratio between the two dispersive terms.

contribution coming from the deviation of the mesoscopic diffusion-dispersion tensor.

Numerical solutions of the closure problem given by Eqs. (58)–(61) are obtained for hierarchical bidisperse porous structures. First, the longitudinal component of the effective diffusion-dispersion coefficient for an inline bidisperse structure is represented in Fig. 6. It is observed that whatever the ratio l_β/l_α, the decrease of the mesoscopic average properties (ε_α and $\mathbf{K}_\alpha^*$) increases the tortuous effect in the diffusive regime (small Péclet numbers), but also gives rise to a more intense dispersion at larger Péclet. In the case of staggered bidisperse structures (Fig. 7), the transition between the diffusive and the dispersive regimes takes place at larger Péclet numbers (transition $\mathrm{Pe}_\beta \sim 10$) than for inline structures (transition $\mathrm{Pe}_\beta \sim 1$). Finally, it can be verified that in the limit where the mesoscopic permeability is high, the macroscopic effective properties tends to the case where the β-region is fluid. Note that at scale I, the relevant nondimensional parameter related to mass transport is the *macroscopic* Péclet number defined as

$$\mathrm{Pe}_\beta = \frac{\|v_\beta\| l_\beta}{\mathcal{D}_{A\alpha}}. \tag{64}$$

In order to evaluate the relative contribution of the additional dispersion present in Eq. (63), the different terms of the effective diffusion-dispersion coefficient are plotted in Fig. 8 for a bidisperse inline structure of scale ratio $l_\beta/l_\alpha = 10$. As expected, it is shown that both the convective contribution $\langle \tilde{\mathbf{v}}_\beta \mathbf{d}_\beta \rangle$ and the extra macroscopic diffusion term $\langle \tilde{\mathbf{D}}_{A\alpha}^* \cdot \nabla \mathbf{d}_\beta \rangle$, strongly depend on the Péclet number. However, because the physical origin of the two terms is different, their dependence on the Péclet and on the microstructure is not the same. This can be clearly observed in Fig. 8(c), where the ratio between the two terms reaches a local minimum at $\mathrm{Pe}_\beta \sim 10^2$ for small $\mathbf{K}_\alpha^*$. For higher values of the mesoscopic permeability, the additional dispersive term gains in importance, before decreasing as the β-region tends to a fluid behavior.

Note that the above observations are in agreement with Moutsopoulos and Koch [7]; however, the present analysis provides a more general and explicit formulation, able to quantify the influence of the finest porous structure in such a bidisperse configuration.

IV. CONCLUSION

In the present work, momentum transport and species dispersion have been studied in a hierarchical bidisperse porous structure. A general macroscopic model has been developed based on the volume-averaging method, and the closure problems associated with the macroscopic effective transport properties have been derived and solved. The results clearly illustrate the micro and mesoscale influence of the geometry and intensity of the local flow on the effective properties at the macroscopic scale. In particular, it has been shown that: (i) The homogenization of Darcy-Brinkman equation results in a transport equation of the same type, where the effective permeability is an explicit function of the permeabilities arising from the micro- and the mesoscopic structure [Eq. (44)]. (ii) Dispersive phenomena at the mesoscopic scale can be dealt with the introduction of a spatial deviation of the diffusion-dispersion tensor, leading to the presence of an additional term in the macroscopic effective tensor [Eq. (63)]. (iii) The mesoscopic dispersion plays a nonnegligible role for moderate scale separations and for low mesoscopic permeability. Moreover, the evaluation of the corresponding additional term tends to diminish the effective macroscopic dispersion.

Although here, for feasibility purpose, the numerical efforts have been focused on simple two-dimensional geometries, the model can be easily applied to more complicated three-dimensional structures. The influence of the mesoscopic dispersion are expected to be important for structures at the mesoscale where large velocity gradients are encountered (for instance concave geometries).

This analysis could be easily extended to more complex hierarchical porous media such as bioreactors for tissue engineering [34].

APPENDIX A: VOLUME-AVERAGING DEFINITIONS

Let us consider a physical quantity Ψ_α associated to the α-phase in the averaging volume $\mathcal{V}_{\mathrm{III}}$ (Fig. 1), the *superficial* volume average of Ψ_α is defined by

$$\langle \Psi_\alpha \rangle = \frac{1}{\mathcal{V}_{\mathrm{III}}} \int_{V_\alpha} \Psi_\alpha(\mathbf{x}+\mathbf{y})\, dV. \tag{A1}$$

Sometimes, the *intrinsic* phase average of Ψ_α is more representative and is defined by

$$\langle \Psi_\alpha \rangle^\alpha = \frac{1}{V_\alpha} \int_{V_\alpha} \Psi_\alpha(\mathbf{x}+\mathbf{y})\, dV. \tag{A2}$$

The two above-averaged values are related by

$$\langle \Psi_\alpha \rangle = \varepsilon_\alpha \langle \Psi_\alpha \rangle^\alpha, \tag{A3}$$

where ε_α is the α-phase volume fraction (porosity).

Finally, averaged conservation equations can be obtained by using spatial and temporal partial derivative theorems given by [13]

$$\langle \nabla \Psi_\alpha \rangle = \nabla \langle \Psi_\alpha \rangle + \frac{1}{\mathcal{V}_{\mathrm{III}}} \int_{A_{\alpha\kappa}} \mathbf{n}_{\alpha\kappa} \Psi_\alpha dA, \tag{A4}$$

$$\left\langle \frac{\partial \Psi_\alpha}{\partial t} \right\rangle = \frac{\partial \langle \Psi_\alpha \rangle}{\partial t} - \frac{1}{\mathcal{V}_{\mathrm{III}}} \int_{A_{\alpha\kappa}} \mathbf{n}_{\alpha\kappa} \cdot \mathbf{w}_{\alpha\kappa} \Psi_\alpha dA, \tag{A5}$$

where $\mathbf{w}_{\alpha\kappa}$ is the interface velocity and $\mathbf{n}_{\alpha\kappa}$ is the unit normal vector at the interface.

APPENDIX B: DERIVATION OF THE MACROSCOPIC SOLUTE TRANSPORT EQUATION

The macroscopic solute transport equation is derived by averaging the mesoscopic equation [Eq. (27)] with the associated boundary condition [Eq. (31)]. The difficulty here lies in the fact that the diffusion-dispersion tensor $\mathbf{D}_{A\alpha}^*$ depends on the velocity field. Let us focus our attention on averaging the right-hand side of Eq. (27). Applying the averaging theorems gives

$$\langle \nabla \cdot (\mathbf{D}^*_{A\alpha} \cdot \nabla c_{A\beta}) \rangle = \nabla \cdot \langle \mathbf{D}^*_{A\alpha} \cdot \nabla c_{A\beta} \rangle + \frac{1}{\mathcal{V}_{\text{II}}} \int_{A_{\beta\sigma}} \mathbf{n}_{\beta\sigma} \cdot (\mathbf{D}^*_{A\alpha} \cdot \nabla c_{A\beta}) dA, \tag{B1}$$

where the area integral is discarded due to the boundary condition [Eq. (31)]. Following Quintard and Whitaker [18], the tensor $\mathbf{D}^*_{A\alpha}$ can be decomposed under the form

$$\mathbf{D}^*_{A\alpha} = \langle \mathbf{D}^*_{A\alpha} \rangle^\beta + \tilde{\mathbf{D}}^*_{A\alpha}, \tag{B2}$$

and also using the spatial decomposition for the concentration $c_{A\beta}$ gives

$$\langle \mathbf{D}^*_{A\alpha} \cdot \nabla c_{A\beta} \rangle = \langle \langle \mathbf{D}^*_{A\alpha} \rangle^\beta \cdot \nabla \langle c_{A\beta} \rangle^\beta + \langle \mathbf{D}^*_{A\alpha} \rangle^\beta \cdot \nabla \tilde{c}_{A\beta} + \tilde{\mathbf{D}}^*_{A\alpha} \cdot \nabla \langle c_{A\beta} \rangle^\beta + \tilde{\mathbf{D}}^*_{A\alpha} \cdot \nabla \tilde{c}_{A\beta} \rangle. \tag{B3}$$

Here, due to scale separation, it can be shown that averaged quantities used in the spatial decomposition are close to averaged quantities defined at the centroid of the averaging volume. Under these circumstances, variation of the averaged quantities can be neglected and the above expression takes the form

$$\langle \mathbf{D}^*_{A\alpha} \cdot \nabla c_{A\beta} \rangle = \langle \mathbf{D}^*_{A\alpha} \rangle^\beta \cdot \langle \nabla \langle c_{A\beta} \rangle^\beta \rangle + \langle \mathbf{D}^*_{A\alpha} \rangle^\beta \cdot \langle \nabla \tilde{c}_{A\beta} \rangle + \langle \tilde{\mathbf{D}}^*_{A\alpha} \cdot \nabla \langle c_{A\beta} \rangle^\beta \rangle + \langle \tilde{\mathbf{D}}^*_{A\alpha} \cdot \nabla \tilde{c}_{A\beta} \rangle. \tag{B4}$$

Let us first consider the third term of Eq. (B4). Using the spatial averaging theorem in the form

$$\nabla \langle c_{A\beta} \rangle^\beta = \langle \nabla c_{A\beta} \rangle^\beta - \frac{1}{V_\beta} \int_{\beta\sigma} \mathbf{n}_{\beta\sigma} c_{A\beta} dA, \tag{B5}$$

allows us to write

$$\langle \tilde{\mathbf{D}}^*_{A\alpha} \cdot \nabla \langle c_{A\beta} \rangle^\beta \rangle = \left\langle \tilde{\mathbf{D}}^*_{A\alpha} \cdot \langle \nabla c_{A\beta} \rangle^\beta - \tilde{\mathbf{D}}^*_{A\alpha} \cdot \frac{1}{V_\beta} \int_{A_{\beta\sigma}} \mathbf{n}_{\beta\sigma} c_{A\beta} dA \right\rangle, \tag{B6}$$

which can also be written under the form

$$\langle \tilde{\mathbf{D}}^*_{A\alpha} \cdot \nabla \langle c_{A\beta} \rangle^\beta \rangle = \langle \tilde{\mathbf{D}}^*_{A\alpha} \rangle \cdot \langle \nabla c_{A\beta} \rangle^\beta - \langle \tilde{\mathbf{D}}^*_{A\alpha} \rangle \cdot \frac{1}{V_\beta} \int_{A_{\beta\sigma}} \mathbf{n}_{\beta\sigma} c_{A\beta} dA. \tag{B7}$$

However, since

$$\langle \tilde{\mathbf{D}}^*_{A\alpha} \rangle = 0, \tag{B8}$$

Eq. (B4) simplifies under the form

$$\langle \mathbf{D}^*_{A\alpha} \cdot \nabla c_{A\beta} \rangle = \langle \mathbf{D}^*_{A\alpha} \rangle^\beta \cdot \langle \nabla \langle c_{A\beta} \rangle^\beta \rangle + \langle \mathbf{D}^*_{A\alpha} \rangle^\beta \cdot \langle \nabla \tilde{c}_{A\beta} \rangle + \langle \tilde{\mathbf{D}}^*_{A\alpha} \cdot \nabla \tilde{c}_{A\beta} \rangle. \tag{B9}$$

Let us consider now the first term of the right-hand side of Eq. (B9). Using the spatial averaging theorem gives

$$\langle \mathbf{D}^*_{A\alpha} \rangle^\beta \cdot \langle \nabla \langle c_{A\beta} \rangle^\beta \rangle = \langle \mathbf{D}^*_{A\alpha} \rangle^\beta \cdot \left[\nabla (\varepsilon_\beta \langle c_{A\beta} \rangle^\beta) + \frac{1}{\mathcal{V}_{\text{II}}} \int_{A_{\beta\sigma}} \mathbf{n}_{\beta\sigma} \langle c_{A\beta} \rangle^\beta dA \right]. \tag{B10}$$

Again, due to scale separation, the above expression becomes

$$\langle \mathbf{D}^*_{A\alpha} \rangle^\beta \cdot \langle \nabla \langle c_{A\beta} \rangle^\beta \rangle = \varepsilon_\beta \langle \mathbf{D}^*_{A\alpha} \rangle^\beta \cdot \nabla \langle c_{A\beta} \rangle^\beta. \tag{B11}$$

The second term of Eq. (B9),

$$\langle \mathbf{D}^*_{A\alpha} \rangle^\beta \cdot \langle \nabla \tilde{c}_{A\beta} \rangle = \langle \mathbf{D}^*_{A\alpha} \rangle^\beta \cdot \left[\nabla \langle \tilde{c}_{A\beta} \rangle + \frac{1}{\mathcal{V}_{\text{II}}} \int_{A_{\beta\sigma}} \mathbf{n}_{\beta\sigma} \tilde{c}_{A\beta} dA \right], \tag{B12}$$

and discarding the average of the deviation, Eq. (B9) finally reduces to

$$\langle \mathbf{D}^*_{A\alpha} \cdot \nabla c_{A\beta} \rangle = \langle \mathbf{D}^*_{A\alpha} \rangle^\beta \cdot \left(\varepsilon_\beta \nabla \langle c_{A\beta} \rangle^\beta + \frac{1}{\mathcal{V}_{\text{II}}} \int_{A_{\beta\sigma}} \mathbf{n}_{\beta\sigma} \tilde{c}_{A\beta} dA \right) + \langle \tilde{\mathbf{D}}^*_{A\alpha} \cdot \nabla \tilde{c}_{A\beta} \rangle. \tag{B13}$$

Finally, the nonclosed averaged equation for solute transport takes the form

$$\varepsilon_\alpha \frac{\partial (\varepsilon_\beta \langle c_{A\beta} \rangle^\beta)}{\partial t} + \varepsilon_\beta \langle \mathbf{v}_\beta \rangle^\beta \cdot \nabla \langle c_{A\beta} \rangle^\beta = \nabla \cdot \left[\langle \mathbf{D}^*_{A\alpha} \rangle^\beta \cdot \left(\varepsilon_\beta \nabla \langle c_{A\beta} \rangle^\beta + \frac{1}{\mathcal{V}_{\text{II}}} \int_{A_{\beta\sigma}} \mathbf{n}_{\beta\sigma} \tilde{c}_{A\beta} dA \right) \right] + \nabla \cdot \langle \tilde{\mathbf{D}}^*_{A\alpha} \cdot \nabla \tilde{c}_{A\beta} \rangle - \nabla \cdot \langle \tilde{\mathbf{v}}_\beta \tilde{c}_{A\beta} \rangle. \tag{B14}$$

APPENDIX C: DEVIATION PROBLEM

The deviation equation is obtained by subtracting the nonclosed Eq. (B14) from the local one [Eq. (4)], where the spatial decompositions have been previously introduced. After a few simplifications, the concentration deviation equation takes the form

$$\tilde{\mathbf{v}}_\beta \cdot \nabla \langle c_{A\beta} \rangle^\beta + \mathbf{v}_\beta \cdot \nabla \tilde{c}_{A\beta} = \nabla \cdot (\mathbf{D}^*_{A\alpha} \cdot \nabla \tilde{c}_{A\beta}) + \nabla \cdot (\tilde{\mathbf{D}}^*_{A\alpha} \cdot \nabla \langle c_{A\beta} \rangle^\beta) - \nabla \cdot \left(\langle \mathbf{D}^*_{A\alpha} \rangle^\beta \cdot \frac{1}{V_\beta} \int_{A_{\beta\sigma}} \mathbf{n}_{\beta\sigma} \tilde{c}_{A\beta} dA \right) - \varepsilon_\beta^{-1} \nabla \cdot \langle \tilde{\mathbf{D}}^*_{A\alpha} \cdot \nabla \tilde{c}_{A\beta} \rangle. \tag{C1}$$

An estimate of the order of magnitude of the different terms of the above deviation equation is preformed in order to simplify the problem. Using the boundary condition Eq. (31) gives

$$-\mathbf{n}_{\beta\sigma} \cdot (\langle \mathbf{D}^*_{A\alpha} \rangle^\beta \cdot \nabla c_{A\beta}) = \mathbf{n}_{\beta\sigma} \cdot (\tilde{\mathbf{D}}^*_{A\alpha} \cdot \nabla c_{A\beta}) \quad \text{at } A_{\beta\sigma}, \tag{C2}$$

where we can deduce that $\langle \mathbf{D}^*_{A\alpha} \rangle^\beta$ and $\tilde{\mathbf{D}}^*_{A\alpha}$ are of the same order of magnitude. Moreover, on the basis of these estimates,

$$\nabla \cdot (\mathbf{D}^*_{A\alpha} \cdot \nabla \tilde{c}_{A\beta}) = \mathcal{O}\left(\frac{\langle \mathbf{D}^*_{A\alpha} \rangle^\beta \tilde{c}_{A\beta}}{l_\beta^2} \right), \tag{C3}$$

$$\nabla \cdot \left(\langle \mathbf{D}^*_{A\alpha} \rangle^\beta \cdot \frac{1}{V_\beta} \int_{A_{\beta\sigma}} \mathbf{n}_{\beta\sigma} \tilde{c}_{A\beta} dA \right) = \mathcal{O}\left(\frac{\varepsilon_\beta^{-1} \langle \mathbf{D}^*_{A\alpha} \rangle^\beta \tilde{c}_{A\beta}}{l_\beta L_{\text{II}}} \right), \tag{C4}$$

$$\varepsilon_\beta^{-1} \nabla \cdot \langle \tilde{\mathbf{D}}^*_{A\alpha} \cdot \nabla \tilde{c}_{A\beta} \rangle = \mathcal{O}\left(\frac{\langle \mathbf{D}^*_{A\alpha} \rangle^\beta \tilde{c}_{A\beta}}{l_\beta L_{\text{II}}} \right), \tag{C5}$$

the two last terms of Eq. (C1) can be discarded and therefore the deviation problem for mass transport takes the form

$$\tilde{\mathbf{v}}_\beta \cdot \nabla \langle c_{A\beta} \rangle^\beta + \mathbf{v}_\beta \cdot \nabla \tilde{c}_{A\beta} = \nabla \cdot (\mathbf{D}^*_{A\alpha} \cdot \nabla \tilde{c}_{A\beta}) + \nabla \cdot (\tilde{\mathbf{D}}^*_{A\alpha} \cdot \nabla \langle c_{A\beta} \rangle^\beta) \tag{C6}$$

$$-\mathbf{n}_{\beta\sigma} \cdot (\mathbf{D}^*_{A\alpha} \cdot \nabla \tilde{c}_{A\beta}) = \mathbf{n}_{\beta\sigma} \cdot (\mathbf{D}^*_{A\alpha} \cdot \nabla \langle c_{A\beta} \rangle^\beta) \quad \text{at } A_{\beta\sigma}. \tag{C7}$$

[1] M. Mota, J. A. Teixeira, W. R. Bowen, and A. Yelshin, Binary spherical particle mixed beds: Porosity and permeability relationship measurement, Trans. Filtr. Soc. **1**, 101 (2001).

[2] M. J. MacDonald, C.-F. Chu, P. P. Guilloit, and K. M. Ng, A generalized blake-kozeny equation for multisized spherical particles, AIChE J. **37**, 1583 (1991).

[3] R. P. Dias, C. S. Fernandes, J. A. Teixeira, M. Mota, and A. Yelshin, Permeability analysis in bisized porous media: Wall effect between particles of different size, J. Hydrol. **349**, 470 (2008).

[4] M. R. Morad and A. Khalili, Transition layer thickness in a fluid-porous medium of multisized spherical beads, Exp. Fluids **46**, 323 (2009).

[5] E. Guyon, L. Oger, and T. J. Plona, Transport properties in sintered porous media composed of two particle sizes, J. Phys. D: Appl. Phys. **20**, 1637 (1987).

[6] H. Vahedi Tafreshi, M. S. A Rahman, S. Jaganathan, Q. Wang, and B. Pourdeyhimi, Analytical expressions for predicting permeability of bimodal fibrous porous media, Chem. Eng. Sci. **64**, 1154 (2009).

[7] K. N. Moutsopoulos and D. L. Koch, Hydrodynamic and boundary-layer dispersion in bidisperse porous media, J. Fluid Mech. **385**, 359 (1999).

[8] K. N. Moutsopoulos, I. N. E. Papaspyros, and V. A. Tsihrintzis, Experimental investigation of inertial flow processes in porous media, J. Hydrol. **374**, 242 (2009).

[9] A. Burghardt, J. Rogut, and J. Gotkowska, Diffusion coefficients in bidisperse porous structures, Chem. Eng. Sci. **43**, 2463 (1988).

[10] J. H. Petropoulos, J. K. Petrou, and A. I. Liapis, Network model investigation of gas transport in bidisperse porous adsorbents, Industr. Eng. Chem. Res. **30**, 1281 (1991).

[11] J. C. Silva and A. E. Rodrigues, Analysis of ZLC technique for diffusivity measurements in bidisperse porous adsorbent pellets, Gas Separat. Purificat. **10**, 207 (1996).

[12] B. Markicevic and N. Djilali, Two-scale modeling in porous media: Relative permeability predictions, Phys. Fluids **18**, 033101 (2006).

[13] S. Whitaker, *The Method of Volume Averaging*, Theory and Applications of Transport in Porous Media (Kluwer Academic Publishers, Dordrecht, 1999).

[14] M. Quintard and S. Whitaker, Transport in chemically and mechanically heterogeneous porous media: II. comparison with numerical experiments for slightly compressible single-phase flow, Adv. Water Res. **19**, 49 (1996).

[15] M. Quintard and S. Whitaker, Transport in chemically and mechanically heterogeneous porous media: I. theoretical development of region-averaged equations for slightly compressible single-phase flow, Adv. Water Res. **19**, 29 (1996).

[16] M. Quintard and S. Whitaker, Transport in chemically and mechanically heterogeneous porous media: III. large-scale mechanical equilibrium and the regional form of Darcys law, Adv. Water Res. **21**, 617(1998).

[17] F. Golfier, D. Lasseux, and M. Quintard, Investigation of the effective permeability of vuggy or fractured porous media from a Darcy-Brinkman approach, Comput. Geosci. **19**, 63 (2014).

[18] M. Quintard and S. Whitaker, Transport in chemically and mechanically heterogeneous porous media: IV. large-scale mass equilibrium for solute transport with adsorption, Adv. Water Res. **22**, 33 (1998).

[19] A. Ahmadi, M. Quintard, and S. Whitaker, Transport in chemically and mechanically heterogeneous porous media: V. two-equation model for solute transport with adsorption, Adv. Water Res. **22**, 59 (1998).

[20] M. Quintard, F. Cherblanc, and S. Whitaker, Dispersion in heterogeneous porous media: One-equation non-equilibrium model, Transport Porous Media **44**, 181 (2001).

[21] F. Cherblanc, A. Ahmadi, and M. Quintard, Two-medium description of dispersion in heterogeneous porous media: Calculation of macroscopic properties, Water Res. Res. **39**, 1154 (2003).

[22] S. Whitaker, Flow in porous media i: A theoretical derivation of Darcys law, Transport Porous Media **1**, 3 (1986).

[23] M. Quintard and S. Whitaker, Convection, dispersion, and interfacial transport of contaminants: Homogeneous porous media, Adv. Water Res. **17**, 221 (1994).

[24] P. Bousquet-Melou, B. Goyeau, M. Quintard, F. Fichot, and D. Gobin, Average momentum equation for interdendritic flow in a solidifying columnar mushy zone, Int. J. Heat Mass Transfer **45**, 3651 (2002).

[25] A. Neculae, B. Goyeau, M. Quintard, and D. Gobin, Passive dispersion in dendritic structures, Mater. Sci. Eng. A **323**, 367 (2002).

[26] B. Goyeau, T. Benihaddadene, D. Gobin, and M. Quintard, Numerical calculation of the permeability in a dendritic mushy zone, Metal. Materials Trans. B **30**, 613 (1999).

[27] A. A. Zick and G. M. Homsy, Stokes flow through periodic arrays of spheres, J. Fluid Mech. **115**, 13 (1982).

[28] G. S. Beavers and D. D. Joseph, Boundary conditions at a naturally permeable wall, J. Fluid Mech. **30**, 197 (1967).

[29] J. Ochoa, P. Stroeve, and S. Whitaker, Diffusion and reaction in cellular media, Chem. Eng. Sci. **41**, 2999 (1986).

[30] B. Goyeau, D. Lhuillier, D. Gobin, and M. Velarde, Momentum transport at a fluid-porous interface, Int. J. Heat Mass Transfer **46**, 4071 (2003).

[31] F. J. Valdés-Parada, C. G. Aguilar-Madera, J. A. Ochoa-Tapia, and B. Goyeau, Velocity and stress jump conditions between a porous medium and a fluid, Adv. Water Res. **62**, 327 (2013).

[32] W. G. Gray, A derivation of the equations for multi-phase transport, Chem. Eng. Sci. **30**, 229 (1975).

[33] B. Goyeau, T. Benihaddadene, D. Gobin, and M. Quintard, Averaged momentum equation for flow through a nonhomogenenous porous structure, Transport Porous Media **28**, 19 (1997).

[34] M. Chabanon, Multiscale study of a perfusion bioreactor for bone tissue engineering, Ph.D. thesis, Ecole Centrale Paris, France, 2015.